nature neuroscience

Overexpression of Down syndrome cell adhesion molecule impairs precise synaptic targeting

Vedrana Cvetkovska[1,3], Alexa D Hibbert[1,3], Farida Emran[1] & Brian E Chen[1,2]

Fragile X syndrome is caused by the loss of Fragile X mental retardation protein (FMRP), an RNA-binding protein that suppresses protein translation. We found that FMRP binds to *Down syndrome cell adhesion molecule* (*Dscam*) RNA, a molecule that is involved in neural development and has been implicated in Down syndrome. Elevated Dscam protein levels in FMRP null *Drosophila* and in flies with three copies of the *Dscam* gene both produced specific and similar synaptic targeting errors in a hard-wired neural circuit, which impaired the flies' sensory perception. Reducing Dscam levels in FMRP null flies reduced synaptic targeting errors and rescued behavioral responses. Our results indicate that excess Dscam protein may be a common molecular mechanism underlying altered neural wiring in intellectual disabilities such as Fragile X and Down syndromes.

Down syndrome and Fragile X syndrome are two of the most common causes of intellectual disability[1,2]. A hallmark of both of these syndromes is elevated protein expression. In Down syndrome, this is a consequence of having three copies of chromosome 21 and the extraneous expression of the thousands of genes located there. In Fragile X syndrome, silencing of the *Fragile X mental retardation 1* (*FMR1*) gene leads to the loss of its protein product, FMRP. FMRP binds RNA targets to suppress their protein translation; thus, in Fragile X syndrome, the loss of FMRP results in excessive protein synthesis of the RNAs that would normally be suppressed[2]. Thousands of RNA targets of FMRP have been discovered using high-throughput RNA sequencing or microarray screens in efforts to identify key molecules involved in Fragile X syndrome and autism spectrum disorders[3–5]. However, it is not known whether unregulated expression of specific molecules common to Down syndrome, Fragile X syndrome and autism spectrum disorders might be responsible for their overlapping neural phenotypes.

One RNA target identified in these screens is *Dscam*[4,5]. In humans, *DSCAM* is a large gene (~800 kb) located in the Down syndrome critical region, a 4 Mb region in chromosome 21 that has been implicated in many Down syndrome phenotypes[6–12]. Dscam is an immunoglobulin cell-surface receptor and has conserved functions in neural development across invertebrates and vertebrates, including axon guidance, axonal and dendritic branching and targeting, and synapse maturation[13]. We characterized *Dscam* RNA as a target for protein translation regulation by FMRP in *Drosophila* brains and examined how overexpression of *Drosophila* Dscam protein through gene triplication or loss of translational suppression by FMRP impairs synaptic targeting precision and neural circuit function.

RESULTS

FMRP binds *Dscam* mRNA to suppress its translation

We identified *Dscam* RNA as a target of FMRP by immunoprecipitation of FMRP from *Drosophila* brains (**Fig. 1a**). This RNA-protein interaction was specific for FMRP, as *Dscam* RNA did not immunoprecipitate with ELAV, a different neuronal RNA-binding protein, or from $Fmr1^{null}$ brains (**Fig. 1a**). The *Dscam* mRNA and FMRP interaction was required for the suppression of Dscam protein translation, as Dscam protein expression in $Fmr1^{null}$ mutants was elevated to levels similar to those of flies with three copies of the *Dscam* gene (**Fig. 1b**). Conversely, flies with multiple copies of the *Fmr1* gene overexpressed FMRP and had lower Dscam protein expression than wild-type flies (**Fig. 1b**). Loss of FMRP resulted in large increases in Dscam protein levels and, conversely, even modest increases in FMRP levels decreased Dscam protein expression by approximately 60% (**Fig. 1b**), indicating a tight regulation of Dscam protein translation by FMRP. These results suggest that FMRP suppresses Dscam protein expression at the level of translation, as *Dscam* mRNA levels remained unchanged in FMRP null flies (**Fig. 1c**).

To understand how this regulation of Dscam expression by FMRP is involved in neural wiring, we used the hard-wired mechanosensory neural circuit to quantitatively analyze axonal targeting decisions[14–16] (**Fig. 2**). A single mechanosensory neuron innervates a single bristle on the back of the fly and, as each bristle is uniquely identifiable, the same neuron among different flies can be identified by the location of its corresponding bristle. We focused our analysis on the left and right posterior scutellar (pSc) neurons, and we verified FMRP expression in identified pSc neurons using immunohistochemistry in combination with fluorescent *in situ* hybridization for *Dscam* mRNA (**Fig. 2a–d**). The pSc neuron extends its axon into the CNS and synapses with specific interneurons, giving it a stereotyped and unique axonal arbor (**Fig. 2e**)[14]. To quantify the variability of this synaptic targeting in wild-type flies, we measured the branch lengths and positions of the pSc axonal arbor in 74 wild-type flies and identified a prototypical 'skeleton' comprised of 16 core branches occurring at >80% frequency for primary and secondary branches and >60% frequency for tertiary branches (**Fig. 2f,g**). Wild-type variability was then defined as branching phenotypes that occurred between 10 and 60% frequency, and

[1]Centre for Research in Neuroscience, Research Institute of the McGill University Health Centre, Montréal, Québec, Canada. [2]Departments of Medicine, and Neurology and Neurosurgery, McGill University, Montréal, Québec, Canada. [3]These authors contributed equally to this work. Correspondence should be addressed to B.E.C. (brian.chen@mcgill.ca).

Received 7 November 2012; accepted 10 April 2013; published online 12 May 2013; doi:10.1038/nn.3396

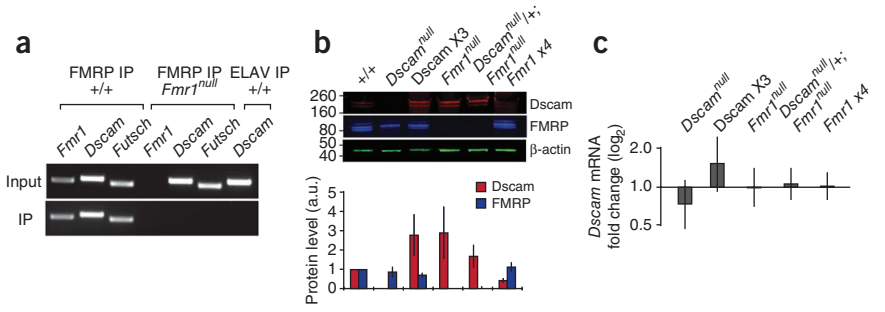

Figure 1 FMRP suppresses Dscam protein translation. (**a**) FMRP binds *Dscam* mRNA. FMRP-mRNA complexes were immunoprecipitated from *Drosophila* larval brains and specific targets were identified by reverse transcription (RT) PCR. FMRP has been previously shown to bind both its own mRNA and *Futsch*. No mRNAs were immunoprecipitated from *Fmr1*^{null} mutants (*Fmr1*^{null} IP), and *Dscam* mRNA did not immunoprecipitate with ELAV, another neuronal RNA-binding protein. (**b**) Loss of FMRP in Fragile X mutants increased neuronal Dscam protein levels. Representative fluorescent immunoblots of Dscam, FMRP and actin in different genotypes are shown. Protein samples for *Dscam*^{null} flies were prepared from embryos and showed restricted expression of FMRP isoforms. Dscam and FMRP protein intensities were normalized to actin (plotted in arbitrary units, a.u.), and the averages from nine experiments are shown. Errors bars represent s.e.m. (**c**) Quantitative real-time PCR analysis revealed that *Dscam* mRNA levels were not significantly altered in *Fmr1*^{null} mutants, $P > 0.05$. *Dscam* mRNA for all experimental genotypes was measured as fold change from wild-type levels. The averages from six experiments are shown. Error bars are s.d. of the mean.

targeting errors were defined as those occurring at <10% in wild-type flies (see Online Methods).

Elevated Dscam levels produce axonal targeting errors

Quantitative analysis of *Fmr1*^{null} flies revealed a significant increase in the total branch length of the pSc axonal arbor ($P < 0.001$), resulting from a significant increase in the number of ectopic branches in the mutants (3.4 branches, $n = 99$ neurons, $P < 0.001$) compared with wild type (1.6 branches, $n = 74$ neurons) (**Fig. 3a**). These increases in axonal arbor sizes in *Fmr1*^{null} mutants were not a result of nonspecific overall growth, as the lengths of the branches that comprised the pSc skeleton were unaffected (**Fig. 3b**). Ectopic branches in the *Fmr1*^{null}

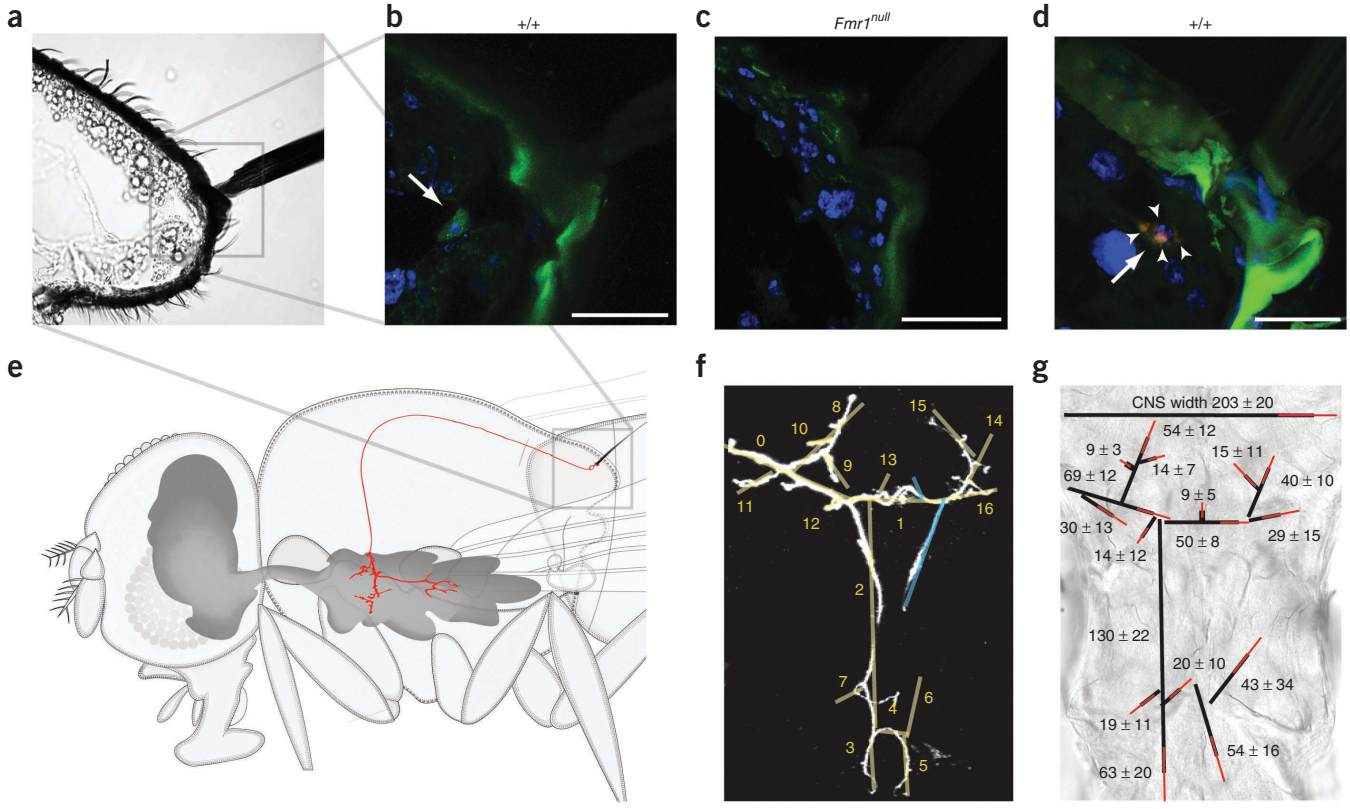

Figure 2 The pSc mechanosensory neuron is identifiable between flies on the basis of the location of its corresponding bristle. (**a**–**d**) The pSc neuron expressed both FMRP and Dscam. A cross section through a pSc bristle is shown in brightfield (**a**), and the corresponding FMRP immunofluorescence (green) within the pSc neuron (arrow) is shown in **b**. No detectable FMRP signal was observed in *Fmr1*^{null} flies (**c**). Colocalization of FMRP and *Dscam* mRNA was observed in pSc neurons using fluorescence *in situ* hybridization for *Dscam* mRNA (magenta) combined with fluorescence immunohistochemistry for FMRP (green) (**d**). Arrowheads point to *Dscam* mRNA puncta, arrow points to FMRP signal. Nuclei are stained in blue. Scale bars represent 20 μm. (**e**) A single mechanosensory neuron innervates a single bristle. The axonal projection into the CNS of the right pSc mechanosensory neuron is shown in red. (**f**,**g**) The stereotyped synaptic connectivity of the pSc neuron was used as a readout for synaptic targeting errors. The wild-type pSc axonal arbor had a complex and stereotyped branching pattern (**f**). Quantitative analysis of wild-type pSc axons revealed 16 core branches (yellow lines) and 2 variable branches occurring in 50% of flies (blue lines). Individual branches of the pSc axonal arbor could be identified between flies, and their lengths and variance were quantified (**g**). Black lines represent the average lengths of each branch, red lines represent the s.d., and values are expressed in μm.

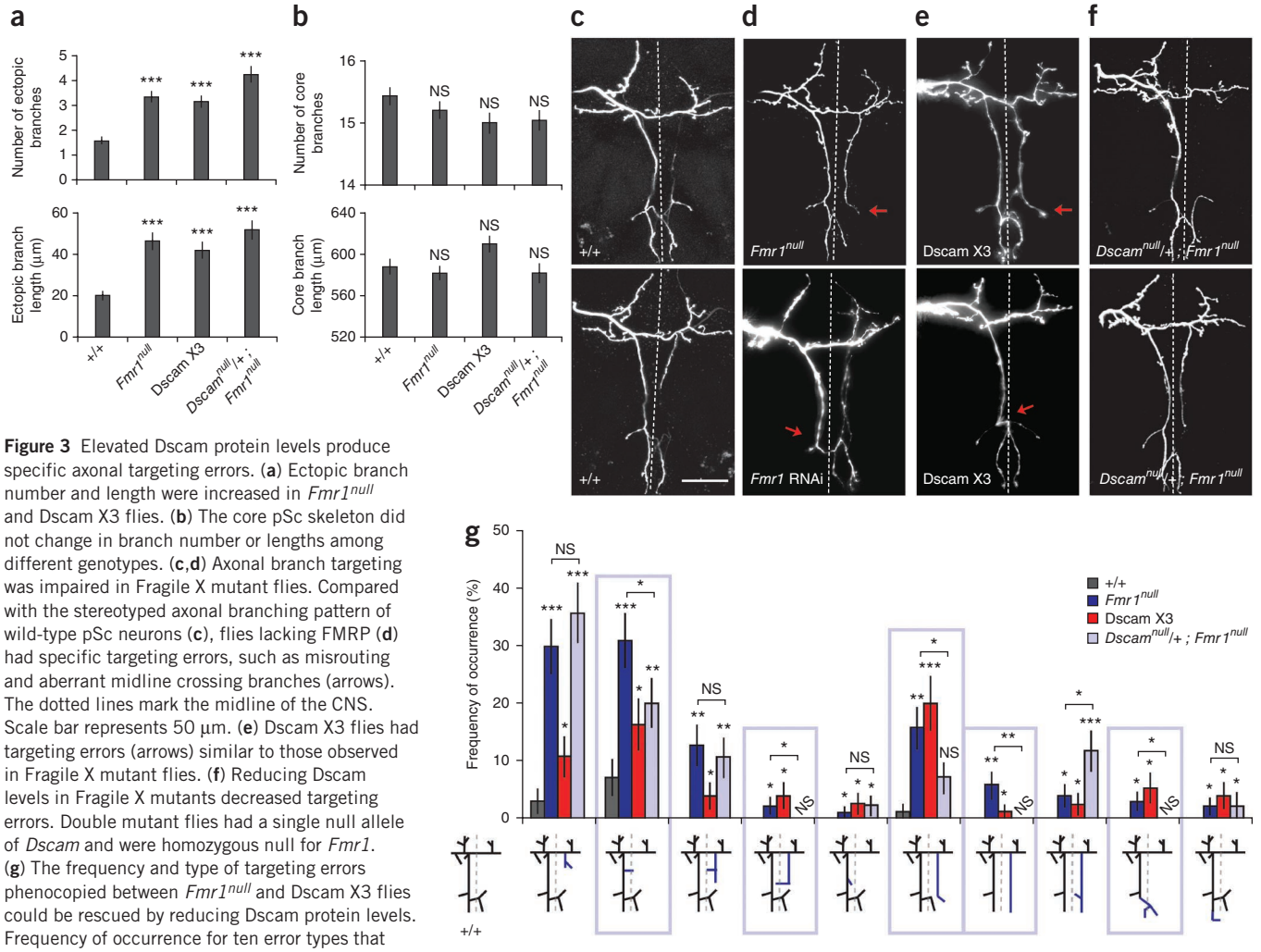

Figure 3 Elevated Dscam protein levels produce specific axonal targeting errors. (**a**) Ectopic branch number and length were increased in *Fmr1*^{null} and Dscam X3 flies. (**b**) The core pSc skeleton did not change in branch number or lengths among different genotypes. (**c**,**d**) Axonal branch targeting was impaired in Fragile X mutant flies. Compared with the stereotyped axonal branching pattern of wild-type pSc neurons (**c**), flies lacking FMRP (**d**) had specific targeting errors, such as misrouting and aberrant midline crossing branches (arrows). The dotted lines mark the midline of the CNS. Scale bar represents 50 μm. (**e**) Dscam X3 flies had targeting errors (arrows) similar to those observed in Fragile X mutant flies. (**f**) Reducing Dscam levels in Fragile X mutants decreased targeting errors. Double mutant flies had a single null allele of *Dscam* and were homozygous null for *Fmr1*. (**g**) The frequency and type of targeting errors phenocopied between *Fmr1*^{null} and Dscam X3 flies could be rescued by reducing Dscam protein levels. Frequency of occurrence for ten error types that were significantly greater than in wild type for both Fragile X mutants and Dscam X3 flies is shown. Double mutant flies had a significant reduction in five axonal targeting errors (purple rectangles). Statistical significance comparisons to wild type are indicated directly above the experimental genotypes' bar; the double mutant comparison to *Fmr1*^{null} flies are indicated above a connecting line. All error bars represent s.e.m. $*P < 0.05$, $**P < 0.01$, $***P < 0.001$, and NS indicates not significant ($P > 0.05$).

flies were highly specific and sprouted at identifiable locations from the prototypical pSc skeleton in the anterior, middle and posterior regions of the CNS (**Fig. 3**). However, Fragile X mutants had many more targeting errors besides ectopic branches, and these errors were also stereotyped and included branch misrouting, midline crossing errors and missing branches from the skeleton (**Fig. 3**). As expected from a total loss of FMRP regulation of many RNA targets, more than 85% of *Fmr1*^{null} flies had targeting errors, with 59% also having multiple errors in their axonal arbors, compared with only 2% of wild-type flies ($P < 0.001$). We confirmed that these errors were a result of the loss of FMRP in mechanosensory neurons by using a specific Gal4 driver (455-Gal4) to express dsRNA specific for *Fmr1* only in the four neurons on the scutellum of the fly[16,17]. Axonal targeting errors in these mosaic flies phenocopied the targeting errors observed in whole fly Fragile X mutants (**Supplementary Fig. 1a**).

Dscam has been shown to be essential in the pSc neuron for axonal branch targeting, but not for the initial axon guidance into the CNS[15]. We confirmed that loss of Dscam in pSc neurons rendered the axonal branches completely incapable of properly targeting in 100% of flies, with axonal branches extending in single directions before curving back onto the primary branch (**Supplementary Fig. 1c**). Thus, given that Dscam is critical for pSc axonal arbor formation and that its protein expression is regulated by FMRP, we sought to examine how axonal targeting is affected solely by increased Dscam protein levels rather than through loss of FMRP suppression. We analyzed the axonal arbors of flies with three copies of the *Dscam* gene (Dscam X3), reflecting the Down syndrome trisomy 21 case. We found that more than 65% of Dscam X3 flies had axonal targeting errors and 30% had multiple errors in their arbors ($n = 74$ neurons, $P < 0.001$ compared with wild type). Similar to Fragile X mutants, Dscam X3 flies also had a significant increase in the number of ectopic branches in their pSc axonal arbors (3.2 ectopic branches per fly, $P < 0.001$; **Fig. 3**). Analysis of the axonal targeting errors in Dscam X3 flies revealed that they were stereotyped and occurred at the same positions as errors observed in the Fragile X mutants (**Fig. 3e**). To measure the degree of overlap in targeting error phenotypes among different genotypes, we performed a blind analysis by shuffling the imaging data from the control and experimental groups (see Online Methods). We categorized 16 different error types among the data, and Fragile X mutants had significantly higher occurrences of all error categories ($P < 0.05$; **Supplementary Fig. 2**). Ten of these errors were found to overlap between Dscam X3

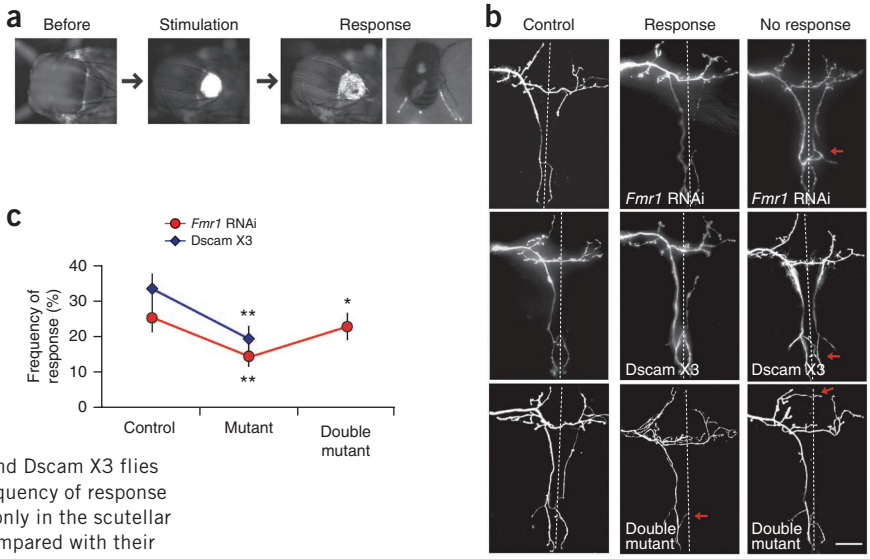

Figure 4 Errors in synaptic targeting impair touch perception. (**a**) Mechanical stimulation of the pSc bristles using a controlled amount of fluorescent dye elicited a cleaning reflex from the rear legs. Transfer of the fluorescent dye from the back of the fly onto the rear legs was used to confirm a positive response. (**b**) Synaptic targeting of a single, identified neuron could be matched to the specific behavioral output for each fly. Representative images of the axonal arbors of previously stimulated pSc neurons are shown. Axonal arbors of mutant flies that either succeeded or failed to respond to bristle stimulation were compared with control responding flies. Arrows indicate targeting errors. The dotted line marks the midline. Scale bar represents 50 µm. (**c**) Synaptic targeting errors in the pSc neuron impaired touch perception in the Fragile X mutant and Dscam X3 flies and could be restored in the double mutant. The frequency of response is shown for mosaic flies with FMRP knocked down only in the scutellar neurons and for flies with three copies of *Dscam*, compared with their specific genetic controls (see Online Methods). The frequency of response to touch in mosaic double mutants, *Dscam*^{null}/*455-Gal4*; *UAS-dsRNA-Fmr1*, was significantly higher than mosaic Fragile X mutants ($P < 0.05$), and was not significantly different from controls ($P > 0.05$, $n > 120$ flies for each genotype). *$P < 0.05$, **$P < 0.01$. Error bars are s.e.m.

and Fragile X mutant flies, and no targeting errors were observed in Dscam X3 flies that did not also occur in Fragile X mutants (**Fig. 3g** and **Supplementary Fig. 2**). These targeting errors were specific for Dscam and Fragile X mutants, as overexpression of other neuronal receptors did not result in these error types and did not produce stereotyped errors (**Supplementary Fig. 3**). Thus, overexpression of Dscam from having three copies of the gene can reproduce a large majority of axonal targeting phenotypes present in Fragile X mutant flies.

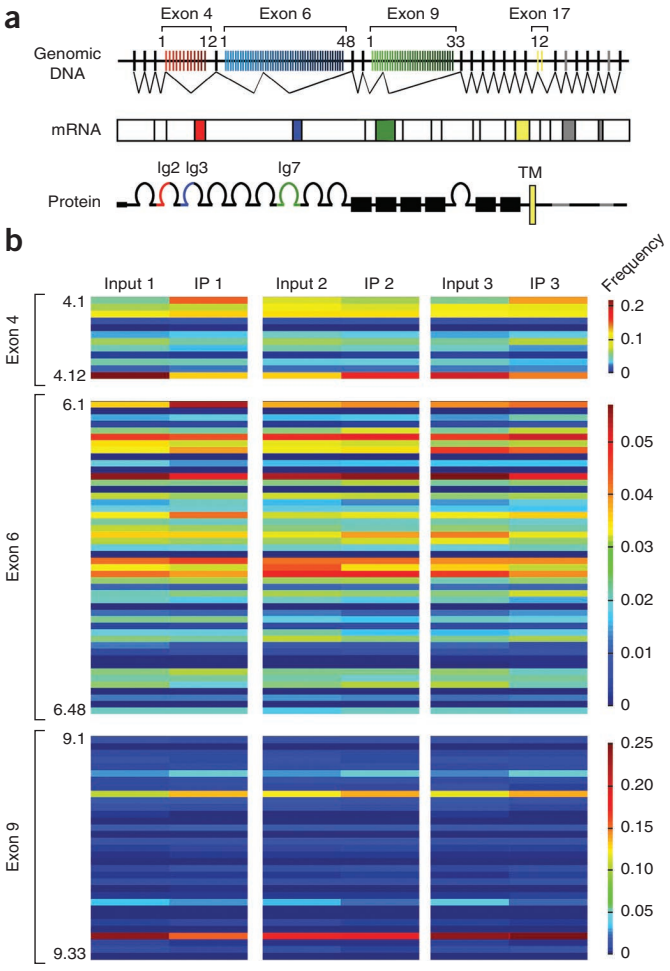

Reducing Dscam levels in Fragile X mutants decreases errors

To determine how Dscam levels contribute to the axonal targeting defects in *Fmr1*^{null} flies, we examined double mutant flies that are heterozygous null for *Dscam* and homozygous null for *Fmr1* (*Dscam*^{null}/+; *Fmr1*^{null}/*Fmr1*^{null}). Removing one copy of the *Dscam* gene reduced Dscam overexpression in *Fmr1*^{null} flies by approximately 40% (**Fig. 1b**). Analysis of the axonal arbors of these *Dscam*^{null}/+; *Fmr1*^{null}/*Fmr1*^{null} double mutant flies (n = 84 neurons) revealed significant reductions in the number of flies with errors (75%) compared with *Fmr1*^{null} flies, and fewer of the double mutants (44%) had multiple errors in their pSc arbors compared with *Fmr1*^{null} flies ($P < 0.05$). We also observed significant reductions in five of the ten phenocopied axonal targeting errors in double mutants compared with *Fmr1*^{null} flies ($P < 0.05$; **Fig. 3g**). However, this also led to a significant increase in one error phenotype, from 4% in *Fmr1*^{null} flies to 12% in double mutants ($P < 0.05$). We therefore conclude that the changes observed

Figure 5 FMRP binds multiple Dscam isoforms. (**a**) Three large arrays of alternatively spliced exons in *Drosophila Dscam* (exon 4, red; exon 6, blue; exon 9, green) encode for different extracellular immunoglobulin domains (Ig2, Ig3 and Ig7). Mutually exclusive splicing from each variable exon can produce 19,008 different extracellular domains. Exon 17 encodes for two alternate transmembrane domains (TM) and exons 19 and 23 can be included or excluded in the intracellular domain. (**b**) High-throughput pyrosequencing of *Dscam* bound to FMRP identified all possible *Dscam* isoforms. *Dscam* isoform distributions from a representative sequencing experiment of >1.2 million reads are shown as heatmaps for variable exons 4, 6 and 9. Isoform distributions from the input and the FMRP immunoprecipitation from three separate experiments are shown. *Dscam* RNA isoforms immunoprecipitated with FMRP showed no substantial bias in representation compared with *Dscam* isoforms in the input fraction, indicating that FMRP bound to all neuronal isoforms equally well.

in these targeting errors represent the axonal targeting decisions that are most sensitive to FMRP regulation of *Dscam*, as the loss of one *Dscam* allele in the Fragile X mutants did not reduce Dscam expression to wild-type levels completely. Furthermore, we observed large variability in Dscam expression at the mRNA and protein levels in both the $Fmr1^{null}$ flies and the double mutants (**Fig. 1b**,**c**), indicating FMRP may also indirectly regulate *Dscam* transcription. FMRP has multiple roles in mRNA splicing, processing, localization and stabilization, and this loss of regulation in Fragile X mutants likely results in large heterogeneities in protein expression throughout the nervous system[2,18–21].

Do these axonal targeting errors in single neurons affect the mechanosensory circuit's function? To measure the ability of a fly to perceive mechanical stimulation of its bristles, we developed a behavioral assay by applying a controlled amount of fluorescent dye to stimulate only the left and right posterior scutellar bristles (**Fig. 4a**). Stimulating these bristles evokes a cleaning reflex from the rear legs[22–25], and the fluorescent dye is transferred from the pSc bristles to the legs. Thus, we can combine this behavioral assay with the morphological and genetic analyses to examine how structural changes and axonal routing errors affect circuit function. We accomplished this by correlating behavioral responses with specific synaptic targeting patterns of the pSc neuron in individual flies (**Fig. 4b**). We examined the cleaning responses in mosaic flies that lacked FMRP in only the scutellar neurons (*455-Gal4*; *UAS-dsRNA-Fmr1*) and in Dscam X3 flies and found that the altered synaptic connectivity of the pSc neurons in both of these mutants significantly reduced their cleaning responses compared with control flies (*455-Gal4* control response rate = 26%, $n = 121$; *455-Gal4*; *UAS-dsRNA-Fmr1* response rate = 15%, $n = 139$; $P < 0.01$; wild-type control response rate = 34%, $n = 121$; Dscam X3 response rate = 20%, $n = 120$; $P < 0.01$; **Fig. 4c** and **Supplementary Fig. 4**). Analysis of double mutant Fragile X mosaic flies lacking one copy of *Dscam* ($Dscam^{null}$/*455-Gal4*; *UAS-dsRNA-Fmr1*) revealed that the Dscam reduction had returned the response rate to that of control flies (23% response, $n = 120$, $P < 0.05$), indicating that reduction of Dscam protein levels can not only rescue synaptic targeting errors, but can also restore touch perception in Fragile X mutant flies.

FMRP binds multiple Dscam isoforms

FMRP binds mRNAs in their untranslated regions through RNA secondary structures known as 'kissing complex RNA' (**Supplementary Fig. 5**)[5,26,27]. Notably, alternative splicing of large exon arrays in the *Drosophila Dscam* gene can produce different immunoglobulin domains to create 19,008 different protein isoforms that differ only in their extracellular region (**Fig. 5a**)[28]. To determine whether FMRP binds to all of these multiple *Dscam* mRNA isoforms, we performed high-throughput pyrosequencing of *Dscam* bound to FMRP after immunoprecipitation. Pyrosequencing of *Dscam* enabled deep coverage of more than 1.2 million reads and long base pair read lengths[29]. We confirmed that all possible *Dscam* isoforms expressed in the brain were also identified bound to FMRP (**Fig. 5b**), indicating that FMRP can suppress translation of tens of thousands of different Dscam protein forms. Comparisons of isoform distributions between *Dscam* in the input fraction and *Dscam* immunoprecipitated with FMRP revealed that there was no substantial bias in the isoforms that FMRP bound (**Fig. 5b**).

These results indicate that FMRP regulation of *Dscam* is dependent on the splicing choices made in individual cells rather than through preferentially regulating specific mRNA isoforms. In addition, the specificity and quantitative overlap of the synaptic targeting errors between Dscam X3 and Fragile X mutants suggest that the effects of Dscam protein overexpression are most likely independent of Dscam isoform choice. Isoform-specific homophilic interactions of the Dscam receptor have been shown to induce dendritic branch repulsion[13], but nearly all of the targeting error phenotypes that we observed in the pSc axons of Dscam X3 and Fragile X mutants consisted of ectopic branches, routing errors and midline crossing errors, indicating an attraction function for the Dscam receptor. Thus, excessive Dscam protein levels in developing axonal branches most likely induces erroneous targeting decisions through inappropriate attraction to cells expressing Dscam ligands.

DISCUSSION

We found that an increase in Dscam protein levels as a result of either three copies of the *Dscam* gene or of a loss of translation suppression by FMRP impaired precise synaptic targeting and neural circuit function. Combining our behavioral analysis of mechanical stimulation of the pSc neuron with pSc axonal targeting patterns, we confirmed that aberrant axonal targeting degrades sensory circuit function at levels appreciable enough to affect the animal's perception. The restoration of the $Dscam^{null}$/+; $Fmr1^{null}/Fmr1^{null}$ double mutants' cleaning response indicates that any other functions of Dscam independent of branch targeting that were impaired in the $Fmr1^{null}$ flies were also rescued. For example, *Aplysia* Dscam is required pre- and postsynaptically for synaptogenesis and synaptic plasticity induction, and Dscam signaling through trans-synaptic complexes leads to the clustering of glutamate receptors[30].

Conversely, overexpression of FMRP may suppress many molecules involved in neural circuit function, such as synaptic transmission. When we overexpressed FMRP in the pSc neuron (*455-Gal4*; *UAS-Fmr1*), this resulted in severe axon guidance and misrouting phenotypes, and also reduced the behavioral responses in these flies (**Supplementary Fig. 6**). Although the axon guidance and misrouting defects were suppressed when combined with Dscam overexpression (*455-Gal4*; *UAS-Fmr1*/$Dscam^{BAC}$), the impaired behavioral response resulting from FMRP overexpression was not restored.

It is important to note that, although the majority of the targeting errors that were phenocopied between Dscam X3 and $Fmr1^{null}$ mutants consisted of ectopic branches, four of the five targeting errors rescued in the double mutant $Dscam^{null}$/+; $Fmr1^{null}/Fmr1^{null}$ flies were errors in branch routing and midline crossing (**Fig. 3g**). However, correlating specific synaptic targeting decisions with an individual fly's behavioral output requires much larger data sets than those generated here, given that we condensed all behavioral positive responses together into a 'yes response' rather than separating the positive responses into different levels of efficiency in removing the fluorescent dye from the scutellum. The highly conserved core 16 skeletal branches observed in almost all pSc neurons are most likely the minimal aspects required for a basic cleaning response.

Although our results indicate that FMRP can bind all *Dscam* isoforms, pyrosequencing of *Dscam* mRNA isoforms in $Fmr1^{null}$ flies revealed specific differences in isoform splicing compared with wild-type flies (**Supplementary Fig. 5**). This may be a result of the loss of FMRP's direct interaction with pre-mRNAs as an exonic splicing enhancer or through unregulated expression of splicing proteins normally suppressed by FMRP[21,31]. FMRP regulation of *Dscam* splicing may also be used in arthropod immune systems, as *Dscam* is expressed in insect and crustacean immune cells such as hemocytes[32,33], and FMRP is also expressed in hemocyte-derived S2 cells[34,35]. In the arthropod immune system, specific Dscam receptor isoforms bind to different pathogens and become preferentially spliced and upregulated for pathogen clearance[32,33,36], but it remains unclear how the feedback

to splicing and expression of Dscam isoforms occurs. FMRP might therefore regulate *Dscam* isoform splicing in many different cell types for a wide range of functions.

We found that neural circuit development and function are sensitive to increases in Dscam protein levels. Previous studies using *Dscam* null heterozygous mice and mouse models of Down syndrome revealed that Dscam dosage is crucial for the proper sorting of retinal ganglion cell axons and dendritic development[12,37], but how Dscam overexpression might contribute to neurological impairments such as Down syndrome has remained unclear. Overexpression of Dscam has also been associated with the congenital heart defects found in Down syndrome, which was identified using analysis of rare individuals with partial duplications of chromosome 21 (ref. 10). Genetic interaction screens in *Drosophila* for congenital heart defect genes also implicated *Dscam*, and overexpression of Dscam in the mouse produced physiological and morphological cardiac defects[38]. Given its evolutionarily conserved widespread functions throughout cardiac and neural development[13] and its conserved interaction with FMRP[4,5], Dscam expression levels are therefore likely to be tightly regulated. Thus, dysregulation of Dscam protein expression may be a common molecular feature underlying a wide variety of neural developmental disorders, such as the dendritic spine pathologies found in Fragile X, Down and Rett syndromes[39–41].

METHODS

Methods and any associated references are available in the online version of the paper.

Note: Supplementary information is available in the online version of the paper.

ACKNOWLEDGMENTS

The authors thank T.-J. Lin, I. Kays and V. Stoudenikina for assistance with experiments, R. Suciu for assistance in pyrosequencing analysis, A. Staffa and the Massively Parallel Sequencing Unit at Génome Québec for pyrosequencing assistance, and B. Douba for graphic arts assistance in the fly drawing. This work was supported by an Alfred P. Sloan Research Fellowship and a Canada Research Chair grant 950-212462 (to B.E.C.) and by funds from the Department of Medicine at McGill University and the Research Institute of the McGill University Health Centre.

AUTHOR CONTRIBUTIONS

B.E.C. designed the experiments and supervised the project. V.C., A.D.H., F.E. and B.E.C. performed the experiments and analyzed the data. V.C., F.E. and B.E.C. wrote the manuscript.

COMPETING FINANCIAL INTERESTS

The authors declare no competing financial interests.

1. Rachidi, M. & Lopes, C. Mental retardation in Down syndrome: from gene dosage imbalance to molecular and cellular mechanisms. *Neurosci. Res.* **59**, 349–369 (2007).
2. Bassell, G.J. & Warren, S.T. Fragile X syndrome: loss of local mRNA regulation alters synaptic development and function. *Neuron* **60**, 201–214 (2008).
3. Ascano, M. Jr. *et al.* FMRP targets distinct mRNA sequence elements to regulate protein expression. *Nature* **492**, 382–386 (2012).
4. Brown, V. *et al.* Microarray identification of FMRP-associated brain mRNAs and altered mRNA translational profiles in fragile X syndrome. *Cell* **107**, 477–487 (2001).
5. Darnell, J.C. *et al.* FMRP stalls ribosomal translocation on mRNAs linked to synaptic function and autism. *Cell* **146**, 247–261 (2011).
6. Takashima, S., Becker, L.E., Armstrong, D.L. & Chan, F. Abnormal neuronal development in the visual cortex of the human fetus and infant with Down's syndrome. A quantitative and qualitative Golgi study. *Brain Res.* **225**, 1–21 (1981).
7. Antonarakis, S.E. 10 years of genomics, chromosome 21 and Down syndrome. *Genomics* **51**, 1–16 (1998).
8. Yamakawa, K. *et al.* DSCAM: a novel member of the immunoglobulin superfamily maps in a Down syndrome region and is involved in the development of the nervous system. *Hum. Mol. Genet.* **7**, 227–237 (1998).
9. Korenberg, J.R. *et al.* Down syndrome phenotypes: the consequences of chromosomal imbalance. *Proc. Natl. Acad. Sci. USA* **91**, 4997–5001 (1994).
10. Barlow, G.M. *et al.* Down syndrome congenital heart disease: a narrowed region and a candidate gene. *Genet. Med.* **3**, 91–101 (2001).
11. Hildmann, T. *et al.* A contiguous 3-Mb sequence-ready map in the S3-MX region on 21q22.2 based on high- throughput nonisotopic library screenings. *Genome Res.* **9**, 360–372 (1999).
12. Alves-Sampaio, A., Troca-Marin, J.A. & Montesinos, M.L. NMDA-mediated regulation of DSCAM dendritic local translation is lost in a mouse model of Down's syndrome. *J. Neurosci.* **30**, 13537–13548 (2010).
13. Schmucker, D. & Chen, B. Dscam and DSCAM: complex genes in simple animals, complex animals yet simple genes. *Genes Dev.* **23**, 147–156 (2009).
14. Ghysen, A. The projection of sensory neurons in the central nervous system of *Drosophila*: choice of the appropriate pathway. *Dev. Biol.* **78**, 521–541 (1980).
15. Chen, B.E. *et al.* The molecular diversity of Dscam is functionally required for neuronal wiring specificity in *Drosophila*. *Cell* **125**, 607–620 (2006).
16. Neufeld, S.Q., Hibbert, A.D. & Chen, B.E. Opposing roles of PlexinA and PlexinB in axonal branch and varicosity formation. *Mol. Brain* **4**, 15 (2011).
17. Hinz, U., Giebel, B. & Campos-Ortega, J.A. The basic-helix-loop-helix domain of *Drosophila* lethal of scute protein is sufficient for proneural function and activates neurogenic genes. *Cell* **76**, 77–87 (1994).
18. Ashley, C.T. Jr., Wilkinson, K.D., Reines, D. & Warren, S.T. FMR1 protein: conserved RNP family domains and selective RNA binding. *Science* **262**, 563–566 (1993).
19. Bagni, C. & Greenough, W.T. From mRNP trafficking to spine dysmorphogenesis: the roots of fragile X syndrome. *Nat. Rev. Neurosci.* **6**, 376–387 (2005).
20. Zalfa, F. *et al.* A new function for the fragile X mental retardation protein in regulation of PSD-95 mRNA stability. *Nat. Neurosci.* **10**, 578–587 (2007).
21. Didiot, M.C. *et al.* The G-quartet containing FMRP binding site in FMR1 mRNA is a potent exonic splicing enhancer. *Nucleic Acids Res.* **36**, 4902–4912 (2008).
22. Canal, I., Acebes, A. & Ferrus, A. Single neuron mosaics of the *Drosophila* gigas mutant project beyond normal targets and modify behavior. *J. Neurosci.* **18**, 999–1008 (1998).
23. Corfas, G. & Dudai, Y. Habituation and dishabituation of a cleaning reflex in normal and mutant *Drosophila*. *J. Neurosci.* **9**, 56–62 (1989).
24. Phillis, R.W. *et al.* Isolation of mutations affecting neural circuitry required for grooming behavior in *Drosophila melanogaster*. *Genetics* **133**, 581–592 (1993).
25. Vandervorst, P. & Ghysen, A. Genetic control of sensory connections in *Drosophila*. *Nature* **286**, 65–67 (1980).
26. Darnell, J.C., Fraser, C.E., Mostovetsky, O. & Darnell, R.B. Discrimination of common and unique RNA-binding activities among Fragile X mental retardation protein paralogs. *Hum. Mol. Genet.* **18**, 3164–3177 (2009).
27. Darnell, J.C. *et al.* Kissing complex RNAs mediate interaction between the Fragile-X mental retardation protein KH2 domain and brain polyribosomes. *Genes Dev.* **19**, 903–918 (2005).
28. Schmucker, D. *et al. Drosophila* Dscam is an axon guidance receptor exhibiting extraordinary molecular diversity. *Cell* **101**, 671–684 (2000).
29. Margulies, M. *et al.* Genome sequencing in microfabricated high-density picolitre reactors. *Nature* **437**, 376–380 (2005).
30. Li, H.L. *et al.* Dscam mediates remodeling of glutamate receptors in Aplysia during *de novo* and learning-related synapse formation. *Neuron* **61**, 527–540 (2009).
31. Guruharsha, K.G. *et al.* A protein complex network of *Drosophila melanogaster*. *Cell* **147**, 690–703 (2011).
32. Watson, F.L. *et al.* Extensive diversity of Ig-superfamily proteins in the immune system of insects. *Science* **309**, 1874–1878 (2005).
33. Watthanasurorot, A., Jiravanichpaisal, P., Liu, H., Soderhall, I. & Soderhall, K. Bacteria-induced Dscam isoforms of the crustacean, *Pacifastacus leniusculus*. *PLoS Pathog.* **7**, e1002062 (2011).
34. Monzo, K. *et al.* Fragile X mental retardation protein controls trailer hitch expression and cleavage furrow formation in *Drosophila* embryos. *Proc. Natl. Acad. Sci. USA* **103**, 18160–18165 (2006).
35. Stetler, A. *et al.* Identification and characterization of the methyl arginines in the fragile X mental retardation protein Fmrp. *Hum. Mol. Genet.* **15**, 87–96 (2006).
36. Dong, Y., Taylor, H. & Dimopoulos, G. AgDscam, a hypervariable immunoglobulin domain–containing receptor of the *Anopheles gambiae* innate immune system. *PLoS Biol.* **4**, e229 (2006).
37. Blank, M. *et al.* The Down syndrome critical region regulates retinogeniculate refinement. *J. Neurosci.* **31**, 5764–5776 (2011).
38. Grossman, T.R. *et al.* Over-expression of DSCAM and COL6A2 cooperatively generates congenital heart defects. *PLoS Genet.* **7**, e1002344 (2011).
39. Dierssen, M. & Ramakers, G.J. Dendritic pathology in mental retardation: from molecular genetics to neurobiology. *Genes Brain Behav.* **5** (suppl. 2), 48–60 (2006).
40. Kaufmann, W.E. & Moser, H.W. Dendritic anomalies in disorders associated with mental retardation. *Cereb. Cortex* **10**, 981–991 (2000).
41. Nimchinsky, E.A., Oberlander, A.M. & Svoboda, K. Abnormal development of dendritic spines in FMR1 knock-out mice. *J Neurosci* **21**, 5139–5146 (2001).

ONLINE METHODS

***Drosophila* strains.** The following *Fmr1*^{null} fly stocks were used and have been verified to lack FMRP (**Fig. 1**)[42–45]: *Fmr1*^{3} (F. Bolduc, University of Alberta), *Fmr1*$^{\Delta 113}$, *Fmr1*$^{\Delta 50M}$ and *Df(3R)Exel6265* (A.P. Haghighi, McGill University). Trans-heterozygous mutant flies were used in experiments (**Supplementary Fig. 7a**) and generated by mating *Fmr1*$^{\Delta 50}$*/TM6b* or *Fmr1*$^{\Delta 113}$*/TM6b* with *Fmr1*^{3}*/TM6*, *Sb*, *Tb* or *Df(3R)Exel6265/TM6b*. To overexpress FMRP, we used flies homozygous for an extra copy of the entire *Fmr1* transcriptional unit, thereby expressing four copies of *Fmr1* (ref. 42). This *Fmr1* genomic fragment was confirmed to rescue FMRP protein expression and the pSc axonal targeting errors in the *Fmr1*^{null} mutants (**Supplementary Fig. 7b**).

Site-specific insertions of a bacterial artificial chromosome (BAC) containing the entire genomic locus of *Dscam* were used to express an extra copy of the *Dscam* gene (H. Bellen, Howard Hughes Medical Institute, Baylor College of Medicine)[46]. Any dominant effects of the BACs were tested by analyzing the pSc axonal arbors in Dscam null flies expressing only the *Dscam* BACs (*Dscam*^{null}*/Dscam*^{null}*; Dscam*^{BAC}; **Supplementary Fig. 8**), and lines *5-*, *7-*, *13-*, *19-*, *20-* and *33-Dscam*^{BAC} were used for experiments. Flies with three copies of *Dscam* were obtained by crossing *Dscam*^{BAC} homozygotes with *w*$^{-}$ flies. *5-Dscam*^{BAC}/+ and *20-Dscam*^{BAC}/+ are shown in **Figure 3e**.

Dscam^{21}*/CyO* and Dscam^{23}*/CyO* (W. Grueber, Columbia University) were used as *Dscam*^{null} mutants[28]. *Dscam*^{null} mutants are embryonic lethal, so *Dscam*^{null} early embryos were collected for negative controls in the immunoblotting experiments[15]. Double mutant flies heterozygous for *Dscam* and homozygous null for *Fmr1* were created by mating *Dscam*^{23}*/CyO; Fmr1*^{3}*/TM6b* to *Fmr1*$^{\Delta 113}$*/TM6b* flies. *Dscam*^{23}/+; *Fmr1*$^{\Delta 50M}$*/Fmr1*^{3} and *Dscam*^{23}/+; *Fmr1*$^{\Delta 113}$*/Fmr1*^{3} are shown in **Figure 3f**.

For RNAi experiments, we used the following *UAS-dsRNA-Fmr1* lines: RNAi lines (*2-1*), (*1-7*) and (*1-10*) (F. Bolduc, University of Alberta)[43], and line 8933 from the Vienna *Drosophila* RNAi Center. Fragile X mutants *Fmr1*$^{\Delta 113}$*/Fmr1*^{3} and *Fmr1*-RNAi^{8933} are shown in **Figure 3d**. Gal4 expression within only the scutellar neurons was achieved using the *455-Gal4* line[16]. To reduce Dscam levels in *Fmr1* RNAi knockdowns, *455-Gal4/CyO; UAS-dsRNA-Fmr1* flies were crossed to *Dscam*^{23}*/CyO; UAS-dsRNA-Fmr1*.

Immunoprecipitation and RT-PCR. Immunoprecipitation experiments were performed in quintuplicate using adult fly brains and verified in sextuplicate from third instar wandering larval brains. FMRP-mRNA complexes were immunoprecipitated from wild-type or *Fmr1*^{null} samples using mouse monoclonal antibody to FMRP (6A15, Abcam) coupled to protein G Dynabeads (Life Technologies). Eluted mRNAs were used as template for RT-PCR using gene-specific reverse transcription primers to *Fmr1* (5′-CTCTCTCCACGCTGCTCATT-3′), *Dscam*(*Exon 11*) (5′-TGATCATAATCACAGCCGAGAGG-3′) and *Futsch* (5′-CTCGCTGGAAGTCTTTGTCC-3′). PCR amplification was performed using forward and reverse primers (respectively for each gene) for *Fmr1* (5′-CGTGCCCGAGAGTATGAAAT-3′, 5′-GTCTCAAAACCGATGTACGC-3′), *Dscam* (5′-CAACGGAGATGTGGTTTCCT-3′, 5′-GGTTATCTCGCTCCCAGACA-3′) and *Futsch* (5′-ATCACCGCAAGTTTTGAAGG-3′, 5′-GCGAAGTCTTTTGGTGCTTC-3′). All other mouse monoclonal antibodies used for immunoprecipitation were obtained from the Developmental Studies Hybridoma Bank. Immunoprecipitation of FMRP-mRNA complexes was also confirmed using another mouse monoclonal antibody, 5B6 (developed by K.S. Broadie, Vanderbilt University). Immunoprecipitation of ELAV-mRNA complexes using the mouse monoclonal antibody 9F8A9 (developed by G.M. Rubin, Janelia Farm Research Campus) and actin complexes using the mouse monoclonal antibody JLA20 (developed by J.J.-C. Lin, University of Iowa) were used as negative controls (**Supplementary Fig. 9**)[47]. ELAV has been shown to extend the 3′ untranslated region of the mRNA *brat*[48], and this was used as a positive control of ELAV-mRNA complex precipitation (**Supplementary Fig. 9**). All antibodies for immunoprecipitation were used at a concentration of 2 mg of antibody per 50 µl of precleared beads.

Pyrosequencing. Immunoprecipitation was performed on adult fly brains using both the 5B6 and 6A15 monoclonal antibodies. Reverse transcription of mRNA extracted from input and immunoprecipitated samples was performed using *Dscam*-specific reverse primers for exons 11 and 7 (5′-CCGCCGATTCCTGGTCGTTTCTTAC). The cDNA was PCR amplified using 454 Lib-L unidirectional sequencing fusion primers containing the 454 adaptor sequence (primer A, forward 5′-CCATCTCATCCCTGCGTGTCTCCGACTCAG-3′; primer B, reverse 5′-CCTATCCCCTGTGTGCCTTGGCAGTCTCAG-3′) and target-specific sequences for exon 4 (forward 5′-AAGCTGGTCTTCCCTCCATT-3′ and reverse 5′-CTCTCCAGAGGGCAATACCA-3′), exon 6 (forward 5′-AGTGCCACAAAAGGACGATT-3′ and reverse 5′-GCTTGTTTACGGGTTGTTCC-3′) and exon 9 (forward 5′-CTACACTTGCGTTGCCAAGA-3′ and reverse 5′-TCAGCCTTGCATTCAACCTT-3′). The PCR products were sequenced using the Roche GS-FLX Titanium sequencer. Samples were prepared in experimental triplicates and pyrosequencing experiments were verified in two sequencing runs. Sequences were analyzed using a custom-written program in MatLab (MathWorks) to distinguish isoforms, and positive identification of isoforms was established for ~70% of sequences. A frequency distribution of isoforms was generated for each exon, experimental replicate and sample. A goodness-of-fit test based on the chi-square distribution was used to calculate statistical significance between frequency distributions of samples. For visual display of isoform frequency distributions, heatmaps were generated using MatLab (MathWorks).

Quantitative real-time PCR. Total RNA was extracted from adult fly heads. Reverse transcription was performed using a *Dscam*-specific reverse primer and a *Ribosomal Protein 49* (*Rp49*)-specific reverse primer (5′-CATCAGATACTGTCCCTTGAAGC-3′). Taqman Fast-Advanced Master Mix (Life Technologies) was used with the following primers and double quenched 5′-FAM/ZEN/IowaBlackFQ-3′ probes (Integrated DNA Technologies): *Rp49* forward 5′-GCGCACCAAGCACTTCATC-3′, *Rp49* probe 5′-FAM-ATATGCTAAGCTGTCGCACAAATGGC-IBFQ-3′, *Rp49* reverse 5′-GACGCACTCTGTTGTCGATACC-3′, *Dscam* forward 5′-ACGATGTAGTTTACAATCAGACAA-3′, *Dscam* probe 5′-FAM-ACCTGCGGGATGAGCTCGGATACA-IBFQ-3′, *Dscam* reverse 5′-GCCTCGCTTAATCCGGTCA-3′. PCR amplification was detected using the Applied Biosystems StepOne Plus Real Time PCR System (Life Technologies) and cycle threshold values were calculated using the StepOne software. Experiments were performed in six experimental replicates with three to six technical replicates. Cycle threshold values were normalized to *Rp49* control levels and technical replicates were averaged within each experimental replicate. *Dscam* mRNA levels from experimental genotypes were compared with wild-type levels from within the same experiment and reported as fold changes from wild type.

Immunoblotting and protein quantification. Immunoblot protein quantification experiments were performed nine times using third instar wandering larval brains and replicated in duplicate in adult brains. Proteins were separated by electrophoresis on a NuPAGE Novex 12% Bis-Tris Gel (Life Technologies) and transferred to a polyvinylidene fluoride membrane. The membrane was incubated with rabbit polyclonal antibody to Dscam (1:1,000, J. Clemens, Purdue University), mouse monoclonal antibody to Fmr1 (1:250, 6A15, Abcam) and mouse monoclonal antibody to actin (1:1,000, C4, CedarLane). For secondary antibodies, we used fluorescent IRDye CW800 antibody to rabbit and antibody to mouse (LI-COR). Proteins were visualized using the Odyssey infrared imaging system (1:10,000, rabbit LIC-926-32211; 1:5,000, mouse LIC-926-32210; LI-COR). Protein bands were quantified by averaging the intensities of five randomly chosen 3 × 3 pixel regions, and Dscam and FMRP levels were normalized to actin.

Immunohistochemistry and fluorescence *in situ* hybridization. Immunohistochemistry experiments on identified mechanosensory neurons were performed 15 times in wild-type, 12 times in *Fmr1*^{null} and 3 times in *Fmr1* RNAi flies. Colabeling of fluorescence *in situ* hybridization for *Dscam* mRNA with fluorescence immunohistochemistry for FMRP in identified pSc neurons was reproduced eight times. Cryosections of the thorax along the rostral-caudal, dorsal-ventral axis were cut at 10 µm thickness from adult female flies. Custom fluorescent RNA probes to *Dscam* were designed to bind all isoforms in the constant mRNA sequences and were conjugated to the Quasar670 dye (Biosearch Technologies). Fluorescence immunohistochemistry with fluorescence *in situ* hybridization was performed as described previously[49]. Mouse monoclonal antibody to FMRP (1:100, 5A11, developed by H. Siomi, Keio University) or mouse monoclonal antibody to FMRP (1:100, 5B6, Life Technologies) was added for

overnight incubation. Alexa Fluor488–conjugated goat antibody to mouse (Life Technologies) was applied during the wash steps, and a Hoechst dye was applied on the final wash to label nuclei.

Fluorescence microscopy was performed using an Olympus laser-scanning confocal microscope FV1000. Images were acquired using a 60× oil objective (NA 1.4). Quantitative analysis of FMRP intensities was performed by measuring the average pixel intensity in the FMRP channel in a region of interest centered around the nucleus of the mechanosensory neuron. The efficiency of the *UAS-dsRNA-Fmr1* was quantified (**Supplementary Fig. 1**) from three experiments and compared with FMRP intensities from wild-type neurons in three experiments.

Carbocyanine dye labeling and imaging. Lipophilic dye labeling of single mechanosensory axons were conducted as previously described[15,16]. The left and right pSc neurons from 2-d-old female flies were labeled with the fluorescent carbocyanine tracers DiI (D282) or DiD (D7757) (Life Technologies) dissolved in ethanol at 20 mg ml^{-1} and 40 mg ml^{-1}, respectively.

The thoracic ganglion was dissected out and slide-mounted with #1 thickness coverslips. Fluorescence and brightfield microscopy was performed using a Zeiss AxioScope A1, or an Olympus laser-scanning confocal microscope FV1000. All images were acquired using a 40× objective (NA 1.0). Image analysis was performed on maximal intensity projections. Transmitted light images were acquired to measure the CNS width and to verify there was no damage to the CNS or occlusions at the surface.

Image analysis. Images were selected for analysis on the basis of low background fluorescence and homogenous and strong labeling throughout a single pSc axon. Images were adjusted for contrast and brightness only. Axonal branch lengths and numbers were measured using a custom-written program in MatLab (MathWorks). For qualitative analysis of pSc axon phenotypes, a prototypical skeleton of the wild-type pSc axonal arbor was first designated by identifying axonal branches that were invariant among 53 w^- neurons. Primary and secondary branches were identified that occurred at greater than 80% frequency and tertiary branches that occurred at greater than 60% frequency. This wild-type pSc skeleton consisted of 16 primary, secondary and tertiary axonal branches ranging from an average of 6 µm for the smallest branch to an average of 130 µm for the largest branch. Branches were considered ectopic if they occurred in less than 10% of wild-type flies. Variable branches were therefore defined as occurring at greater than 10 and less than 60% frequency, with an average frequency of 30% per wild-type fly. The midline was defined as a 10-µm-wide region running along the anterior-posterior axis of the CNS. Any branch entering or crossing this region was considered a midline-crossing branch. The length of the primary axon entry point into the CNS (**Fig. 1c**, 'branch 0') is dependent on the number of images collected above the entry point as the axon travels in its fascicle, and so was not included in the branch length measurement calculations. Axon guidance errors of the primary axon entry point were quantified, but not counted as axonal targeting errors and occurred at 1.1 and 1.4% in $Fmr1^{null}$ and Dscam X3 mutants, respectively, and did not occur in wild-type flies. Branch lengths among all genotypes were normally distributed from their means. One-way ANOVA followed by Dunnett's *post hoc* pairwise comparison was used to determine statistical significance in branch lengths between wild-type and mutant genotypes. For statistical testing of discrete measurements, nonparametric Mann-Whitney *U* test was used to determine statistical significance in branch numbers between wild-type and mutant genotypes.

A total of 74 wild-type, 100 $Fmr1^{null}$, 74 Dscam X3 and 84 $Dscam^{null}$/+; $Fmr1^{null}$ double mutant neurons were analyzed. Sample sizes were chosen on the basis of previous studies[15,16]. Qualitative analysis of axonal targeting variability was performed blind to genotype by shuffling the axonal arbor data among all genotypes, and 28 different targeting variability types were identified. Wild-type variability was identified (12 types) and 16 error types were found with a frequency of less than 10% in wild type, and this was then used as a cutoff for the definition of a targeting error (**Supplementary Fig. 2**). Errors in all 16 categories were found in $Fmr1^{null}$ flies. Dscam X3 flies had errors in 15 categories, but 5 of these 15 error types were not significantly different from wild type ($P > 0.05$); thus, the ten error types significantly higher in both $Fmr1^{null}$ and Dscam X3 mutants compared with wild type were defined as the targeting error phenocopy ($P < 0.05$). Targeting errors were considered to be rescued in the double mutant flies if the error frequency was significantly lower than in the $Fmr1^{null}$ flies. Statistical significance for each category between genotypes was determined by performing multiple comparisons using a two-tailed *t* test for proportions set at $P < 0.05$.

Behavioral analysis. The scutellum-specific Gal4 driver, *455-Gal4*, was used to drive *Fmr1* dsRNA only in the four scutellar mechanosensory neurons to ensure that the rest of the fly, particularly the postsynaptic neural circuitry, was left unperturbed by the gene manipulations. Dual color dye labeling of scutellar neurons and unaffected dorsocentral neurons were performed periodically to ensure specificity of the Gal4 driver[16], and *455-Gal4>Dscam dsRNA* flies, which lack all axonal branch targeting, were used as negative controls[15,16]. Experiments were performed on 2-d-old female flies with the experimenter blind to genotype. All genotypes were assayed on the same day to control for seasonal growth effects, and at the same approximate time (early afternoon) to control for circadian effects. Flies were decapitated and left to recover for 1 h in a humidified chamber. To ensure the integrity of the cleaning reflex circuit, flies were pre-selected by stimulating the notopleural bristles to elicit a cleaning response from the two front legs. The two pSc bristles of decapitated flies were stimulated by pressure injection of fluorescent dye (40 mg ml^{-1} of DiD in ethanol or 2.5 mg ml^{-1} of DiO in dimethylformamide). Success or failure to elicit a cleaning reflex was scored visually and then verified by the transfer of dye to the rear legs of the fly. The pSc bristles were then plucked from both responding and nonresponding flies and the flies were prepared for subsequent dye filling and morphological analysis. A total of 121 w^- controls, 121 *455-Gal4*/+ controls, 125 *UAS-dsRNA-Fmr1* controls, 77 $Dscam^{23}$/+ controls, 120 Dscam X3, 139 *455-Gal4*/+; UAS-*dsRNA-Fmr1* mutants and 120 double mutant ($Dscam^{23}$/*455-Gal4*; *UAS-dsRNA-Fmr1*) flies were analyzed using DiD stimulation (**Supplementary Fig. 4**). Sample sizes were chosen based on previous studies[22–25]. All behavioral results were verified using DiO dissolved in dimethylformamide, a more viscous solvent, to stimulate the pSc bristles which produced greater response rates in all genotypes, and produced identical results among genotypes. Statistical significance in response rate between each genotype was determined using a two-tailed *t* test for proportions set at $P < 0.05$.

42. Dockendorff, T.C. *et al. Drosophila* lacking dfmr1 activity show defects in circadian output and fail to maintain courtship interest. *Neuron* **34**, 973–984 (2002).
43. Bolduc, F.V., Bell, K., Cox, H., Broadie, K.S. & Tully, T. Excess protein synthesis in *Drosophila* fragile X mutants impairs long-term memory. *Nat. Neurosci.* **11**, 1143–1145 (2008).
44. Zhang, Y.Q. *et al. Drosophila* fragile X-related gene regulates the MAP1B homolog Futsch to control synaptic structure and function. *Cell* **107**, 591–603 (2001).
45. Parks, A.L. *et al.* Systematic generation of high-resolution deletion coverage of the *Drosophila melanogaster* genome. *Nat. Genet.* **36**, 288–292 (2004).
46. Venken, K.J., He, Y., Hoskins, R.A. & Bellen, H.J. P[acman]: a BAC transgenic platform for targeted insertion of large DNA fragments in *D. melanogaster*. *Science* **314**, 1747–1751 (2006).
47. Reeve, S.P. *et al.* The *Drosophila* fragile X mental retardation protein controls actin dynamics by directly regulating profilin in the brain. *Curr. Biol.* **15**, 1156–1163 (2005).
48. Hilgers, V., Lemke, S.B. & Levine, M. ELAV mediates 3′ UTR extension in the *Drosophila* nervous system. *Genes Dev.* **26**, 2259–2264 (2012).
49. Raj, A., van den Bogaard, P., Rifkin, S.A., van Oudenaarden, A. & Tyagi, S. Imaging individual mRNA molecules using multiple singly labeled probes. *Nat. Methods* **5**, 877–879 (2008).

doi:10.1038/nn.3396